Response of Thermohaline Circulation to Freshwater Forcing under Present-Day and LGM Conditions

AIXUE HU, BETTE L. OTTO-BLIESNER, AND GERALD A. MEEHL

Climate and Global Dynamics Division, National Center for Atmospheric Research, Boulder, Colorado*

WEIQING HAN

Department of Atmospheric and Oceanic Sciences, University of Colorado, Boulder, Colorado

CARRIE MORRILL

NOAA/NCDC Paleoclimatology Program, and CIRES Climate Diagnostics Center, University of Colorado, Boulder, Colorado

ESTHER C. BRADY AND BRUCE BRIEGLEB

Climate and Global Dynamics Division, National Center for Atmospheric Research, Boulder, Colorado*

(Manuscript received 10 April 2007, in final form 17 October 2007)

ABSTRACT

Responses of the thermohaline circulation (THC) to freshwater forcing (hosing) in the subpolar North Atlantic Ocean under present-day and the last glacial maximum (LGM) conditions are investigated using the National Center for Atmospheric Research Community Climate System Model versions 2 and 3. Three sets of simulations are analyzed, with each set including a control run and a freshwater hosing run. The first two sets are under present-day conditions with an open and closed Bering Strait. The third one is under LGM conditions, which has a closed Bering Strait. Results show that the THC nearly collapses in all three hosing runs when the freshwater forcing is turned on. The full recovery of the THC, however, is at least a century earlier in the open Bering Strait run than the closed Bering Strait and LGM runs. This is because the excessive freshwater is diverged almost equally toward north and south from the subpolar North Atlantic when the Bering Strait is open. A significant portion of the freshwater flowing northward into the Arctic exits into the North Pacific via a reversed Bering Strait Throughflow, which accelerates the THC recovery. When the Bering Strait is closed, this Arctic to Pacific transport is absent and freshwater can only be removed through the southern end of the North Atlantic. Together with the surface freshwater excess due to precipitation, evaporation, river runoff, and melting ice in the closed Bering Strait experiments after the hosing, the removal of the excessive freshwater takes longer, and this slows the recovery of the THC. Although the background conditions are quite different between the present-day closed Bering Strait run and the LGM run, the THC responds to the freshwater forcing added in the North Atlantic in a very similar manner.

1. Introduction

The thermohaline circulation [(THC), or the meridional overturning circulation (MOC)] is a global-scale, three-dimensional oceanic circulation. It transports warmer and saltier upper-ocean water into the subpolar North Atlantic, where that water loses its heat to the atmosphere and becomes cold and dense, then sinks to the deep ocean in the Labrador Sea and the Greenland–Iceland–Norwegian Seas forming the North Atlantic Deep Water. This deep water flows southward and upwells elsewhere in the world's oceans. Dense deep water (called the Antarctic Bottom Water) also forms around the periphery of the Antarctic. The formation of the Antarctic Bottom Water is mainly related to ice–ocean and ice shelf–ocean interactions. Changes

* The National Center for Atmospheric Research is sponsored by the National Science Foundation.

Corresponding author address: Aixue Hu, Climate and Global Dynamics Division, National Center for Atmospheric Research, Boulder, CO 80021.
E-mail: ahu@ucar.edu

DOI: 10.1175/2007JCLI1985.1

in the rate of these two deep water formations are likely associated with hemispheric-scale climate oscillations (e.g., Broecker 1998). Currently, observational studies suggest that the THC transports about 1.2×10^{15} W of heat northward in the Atlantic at 24°N (Ganachaud and Wunsch 2000; Talley et al. 2003). Significant alterations in this circulation could induce dramatic regional and global climate change (e.g., Manabe and Stouffer 1988; Delworth et al. 1993; Timmermann et al. 1998; Vellinga et al. 2001; Stocker 2002; Timmermann et al. 2005a,b; Dahl et al. 2005; Zhang and Delworth 2005; Levermann et al. 2005; Schmittner 2005; Broccoli et al. 2006; Stouffer et al. 2006).

Frequent occurrences of abrupt climate change during the last glacial period have been indicated by paleoclimate studies, for example, the Dansgaard–Oeschger (D–O) events (Dansgaard et al. 1993; Ditlevsen et al. 2005), the Heinrich events (Heinrich 1988; Hemming 2004), and the Younger Dryas (Grootes et al. 1993; Alley et al. 1993; Hemming et al. 2000). These abrupt climate change events have been linked to the shutdown or reestablishment of the THC (e.g., Clark et al. 2002; Rahmstorf 2002). The shutdown of the THC has been attributed to a pulse of glacier meltwater into the Atlantic (e.g., Rahmstorf 1995, 1996; Clark et al. 2002; Clarke et al. 2003; Rahmstorf et al. 2005).

Theoretical and modeling studies indicate that the Bering Strait may play an important role in the response of the THC to freshwater forcings added in the subpolar North Atlantic (Shaffer and Bendtsen 1994; De Boer and Nof 2004a,b; Hu and Meehl 2005a; Hu et al. 2007a, hereafter H07). Presently, the Bering Strait is a narrow and shallow pathway connecting the Pacific and Atlantic Oceans through the Arctic with a maximum width of about 150 km and a depth of about 50 m. Observational studies indicate there is an annual mean throughflow about 0.8 Sv ($1 \text{ Sv} \equiv 10^6 \text{ m}^3 \text{ s}^{-1}$) from the Pacific into the Arctic (e.g., Aagaard and Carmack 1989; Wijffels et al. 1992). However, during much of the last glacial period, this strait was closed because of lower sea level (Sidall et al. 2003). Studies show that the freshwater transported by the Bering Strait Throughflow makes up roughly 30% of the total freshwater into the Arctic under present-day conditions (e.g., Aagaard and Carmack 1989; Woodgate and Aagaard 2005). The subsequent export of this freshwater from the Arctic into the North Atlantic affects the strength of the THC by altering the rate of the North Atlantic deep convection (Reason and Power 1994; Goosse et al. 1997; Wadley and Bigg 2002; Hasumi 2002; Hu and Meehl 2005a; H07), and can also influence the deep western boundary currents in the Atlantic and the separation point of the Gulf Stream from the eastern coast of America (Huang and Schmitt 1993).

A few existing theoretical and coupled model studies suggest that the open/closed Bering Strait can have a strong influence on THC variability. Since the Bering Strait Throughflow is primarily geostrophically controlled (Overland and Roach 1987), Shaffer and Bendtsen (1994) used a three-box THC model and found that both active and collapsed THC modes are stable, steady modes for a closed Bering Strait. With an open Bering Strait, however, when the sea level increases by about 14 m above the present-day level, a stable, active THC is replaced by a collapsed THC caused by an enhanced transport of the North Pacific freshwater into the Arctic and Atlantic. Theoretical studies of De Boer and Nof (2004a,b) pointed out that, under modern climate conditions, there are about 4 Sv of the upper-ocean water forced northward into the South Atlantic by strong Southern Ocean winds. With an active THC, this 4-Sv water would return to the Southern Oceans via the lower branch of the THC as North Atlantic Deep Water. If the THC collapses, this water would exit the Atlantic basin into the Pacific through the open Bering Strait. Consequently, any strong freshwater flux into the North Atlantic that could sufficiently shut down the THC would be quickly flushed out of the North Atlantic into the North Pacific via the Bering Strait, and the THC would be reestablished fairly quickly.

A recent coupled model study of Hu and Meehl (2005a) showed a result consistent with these theoretical works. By analyzing the 1-Sv hosing experiment using the National Center for Atmospheric Research (NCAR) Community Climate System Model version 2 (CCSM2), Hu and Meehl (2005a) suggested that the open Bering Strait may have significant influence on the time scale of the THC recovery after the termination of the additional freshwater flux. H07 further studied the impact of the Bering Strait on the THC's response to freshwater forcing added into the subpolar North Atlantic by comparing two CCSM2 hosing simulations with an open and closed Bering Strait under present-day conditions. They found that the recovery of the THC is delayed by about a century in the closed Bering Strait (CBS) hosing run as compared to the open Bering Strait (OBS) one. This delayed THC recovery is attributed to the closed Bering Strait that prevents the transport of the added freshwater from the North Atlantic into the North Pacific via the Arctic. Instead, the freshwater exported into the Arctic from the North Atlantic during the hosing is transported back to the North Atlantic as sea ice after the hosing, resulting in a higher surface freshwater input in the CBS hosing run, suppressed deep convection, and thus

a delayed recovery of the THC. Therefore, they speculated that, relative to the short-lived 8.2-ka cold event in the early Holocene, the long-lasting abrupt climate change events during the last glacial period, such as the D–O events and the Heinrich events, might be related to the delayed recovery of the THC induced by the closed Bering Strait at that time.

There are many differences between the present-day conditions and the conditions during the last glacial period, such as the orbital forcing and associated solar radiation, land glaciers and ice sheet and associated albedo effects, and atmospheric greenhouse gas concentrations and sea level. These differences may cause different responses of the THC to freshwater forcing added into the subpolar North Atlantic. Since a closed Bering Strait induces a delayed recovery of the THC under present-day conditions (H07), here we further investigate whether this finding would hold under the last glacial maximum (LGM) conditions. Especially, we focus on the differences of the THC response to freshwater forcing between the present-day OBS hosing simulation and the LGM hosing simulation with a closed Bering Strait, and the similarities between the present-day CBS hosing run and the LGM hosing run. The paper is organized as follows: section 2 describes the models and experiment setup, section 3 shows the results, and the conclusion and discussion are given in section 4.

2. Models and experiments

a. Models

The models used in this study are the NCAR CCSM2 (Kiehl and Gent 2004) and CCSM3 (Collins et al. 2006). The atmospheric component in CCSM2 is the NCAR Community Atmosphere Model version 2 (CAM2) using spectral dynamics at T42 resolution and 26 hybrid levels vertically. The ocean model is a version of the Parallel Ocean Program (POP) developed at Los Alamos National Laboratory with 1° horizontal resolution and enhanced meridional resolution (1/2°) in the equatorial tropics and the North Atlantic and with 40 vertical levels. The sea ice model is the Community Sea Ice Model version 4 (CSIM4) with elastic–viscous–plastic dynamics, a subgrid-scale thickness distribution, and energy-conserving thermodynamics. The land model is the Community Land Model version 2 (CLM2).

The component models in the version of CCSM3 used in this study bear the same horizontal and vertical resolutions as those in CCSM2. In comparison with CCSM2, many improved physics and numerics are implemented in each of the component models of CCSM3. The major physical and numerical improvements are 1) a better treatment of the cloud and precipitation processes, radiation processes, and the aerosols and atmospheric dynamics in the Community Atmospheric Model version 3 (CAM3); 2) a more efficient solver for the barotropic continuity equation, a nonuniform absorption of solar radiation based on in situ chlorophyll and satellite ocean color observations (Ohlmann 2003), and a parameterized double diffusive mixing scheme in the ocean component (POP1.4.3); 3) a modified formulation of the biogeophysics to increase the sensible and latent heat fluxes over sparsely vegetated surface, and a scheme to account for the effects of competition for water among plant functional types in the Community Land Model version 3 (CLM3); and 4) modifications to the sea ice dynamics, sea ice albedos, and exchanges of salt between sea ice and the surrounding ocean in Community Sea Ice Model version 5 (CSIM5).

Both versions of the CCSM model produce a stable global mean climate comparable to observations (Kiehl and Gent 2004; Otto-Bliesner et al. 2006; Collins et al. 2006). On the other hand, with all of these improvements in physics and numerics, the simulated climate in the CCSM3 control run under 1990s conditions is better than that in CCSM2 when compared with the observations. The major improvements of the simulated climate in CCSM3 relative to CCSM2 include a reduced cold bias in the polar regions of the upper troposphere and in the tropical tropopause, a better energy balance at both surface and top of the atmosphere, a reduced sea surface temperature and salinity bias in many regions of the World Ocean, a closer to observed Atlantic meridional heat transport, and a better sea ice thickness distribution. A more detailed description of these improvements can be found in Collins et al. (2006) and the references therein.

b. Model setup and experiment design

The CCSM2 is set up under present-day conditions (1990), with an atmospheric CO_2 concentration of 355 ppm, and the CCSM3 is under LGM conditions (about 21 000 yr before present) with an atmospheric CO_2 concentration of 185 ppm. The solar insolation and other greenhouse gases are also adjusted to the LGM value. Since the sea level is about 120 m lower during LGM than in the present day, the coastline and a few key shallow sills are modified according to the LGM fifth global model of the variation of ice thickness over the continents from the LGM to the present (ICE-5G) reconstruction (Peltier and Solheim 2004). The continental ice sheet, which modifies the continental topography and albedo, is also included according to the same reconstruction dataset.

Three sets of experiments are analyzed in this study.

TABLE 1. Information of the control and hosing experiments.

	OBS (CCSM2)	LGM (CCSM3)	CBS (CCSM2)
Period of control experiments	Yr 0–600	Yr 0–230	Yr 100–400
Start year of the hosing experiments	Yr 100	Yr 100	Yr 100
Length of the hosing experiments	450 yr	550 yr	450 yr

Each set includes a control simulation and a freshwater hosing experiment. The first two sets of simulations are under present-day conditions with an open and closed Bering Strait (Hu and Meehl 2005a; H07), and the third set is under LGM conditions with a realistically closed Bering Strait (Otto-Bliesner et al. 2007). The control simulations are simulations with all forcings being held fixed, such as orbital forcing and associated solar radiation at the top of the atmosphere, atmospheric CO_2 concentration, and so on. In the hosing runs, a pulse of freshwater flux (1 Sv) lasting for 100 yr is uniformly distributed into subpolar North Atlantic between 50° and 70°N. Then this additional freshwater forcing is terminated to allow the climate system to recover. This experimental design follows the standard for the THC Coupled Model Intercomparison Project (CMIP) simulations where the freshwater forcing strengths were 0.1 and 1 Sv (Stouffer et al. 2006). Here we use the stronger freshwater forcing case.

The OBS control run is a segment of 600 yr of the CCSM2 millennial present-day control run (Kiehl and Gent 2004). The CBS control run and the two present-day hosing runs are branched at year 100 of this segment. The CBS control run is integrated for 300 yr, and the two hosing runs are integrated for 450 yr. The LGM control run is a segment of 230 yr from the CCSM3 LGM control run (Otto-Bliesner et al. 2006), and the LGM hosing run is branched at year 100 of this segment and lasts for 550 yr (Table 1). In our hosing experiments, the additional freshwater flux is not compensated elsewhere in the World Ocean and the global sea level is not allowed to rise because of this freshwater flux in our models. Thus the dynamic impact of the added freshwater forcing and the associated geostrophic adjustment are not included in the current model experiments. And after the hosing, the global ocean is fresher.

The 1-Sv additional freshwater flux is close to the current global river runoff. A freshwater flux this large is extremely unlikely to happen in the future under realistically projected greenhouse gas forcing, though it could have occurred during the last deglaciation (Yokoyama et al. 2000; Clark and Mix 2000; Clarke et al. 2003; Clark et al. 2004). This flux and its duration might be on the high side of some paleorecords (e.g., Sarnthein et al. 1995), but within the range of the more recent paleoevidence for the last deglacial period (e.g., Yokoyama et al. 2000; Clark and Mix 2000; Clark et al. 2004). These records show that the mean global sea level could have risen by more than 10 m within 100–500 yr (Sidall et al. 2003; Roche et al. 2004), equivalent to a freshwater flux of 0.25–2 Sv into the North Atlantic from the land ice sheet collapse around the North Atlantic region about 19 000 yr ago. A forcing weaker than this shuts down the THC completely in some stand-alone ocean models (e.g., Seidov et al. 1996) and has caused significant weakening of the THC in some coupled models (e.g., Stouffer et al. 2006).

We recognize that two versions of the CCSM model under different climate conditions are used in these hosing experiments. Our results indicate that the effect of the Bering Strait on the response of the THC to freshwater forcing is similar under present-day or the LGM conditions. In addition, these two versions of the CCSM model, at least to some degree, give us a chance to independently test whether the finding of H07 would hold in different models under different climatic background conditions.

3. Model results

a. Response of the THC

The time evolution of the THC strength is given in Fig. 1a. Since the THC dominates the MOC in the Atlantic, the THC index is defined as the maximum value of the Atlantic meridional streamfunction (MSF) below 500 m. The THC index shown in Fig. 1a is normalized by the control mean. The control mean of the maximum THC is 15.6 Sv for present-day OBS simulation, 18.3 Sv for the present-day CBS simulation, and 17 Sv for LGM simulation. The THC strength in these three control runs is within the range of the THC suggested for present day by observations (e.g., McCartney and Talley 1984; Ganachaud and Wunsch 2000). The stronger THC in the CBS control run results from less freshwater export from the Arctic into the North Atlantic, since the closed Bering Strait prevents the transport of the fresher Pacific water into the Arctic and the Atlantic, thus leading to more intensified deep convection in the North Atlantic consistent with previous studies with stand-alone ocean models (Wadley and Bigg 2002; Reason and Power 1994). In CCSM3, the control run THC under LGM conditions is weaker and the overturning

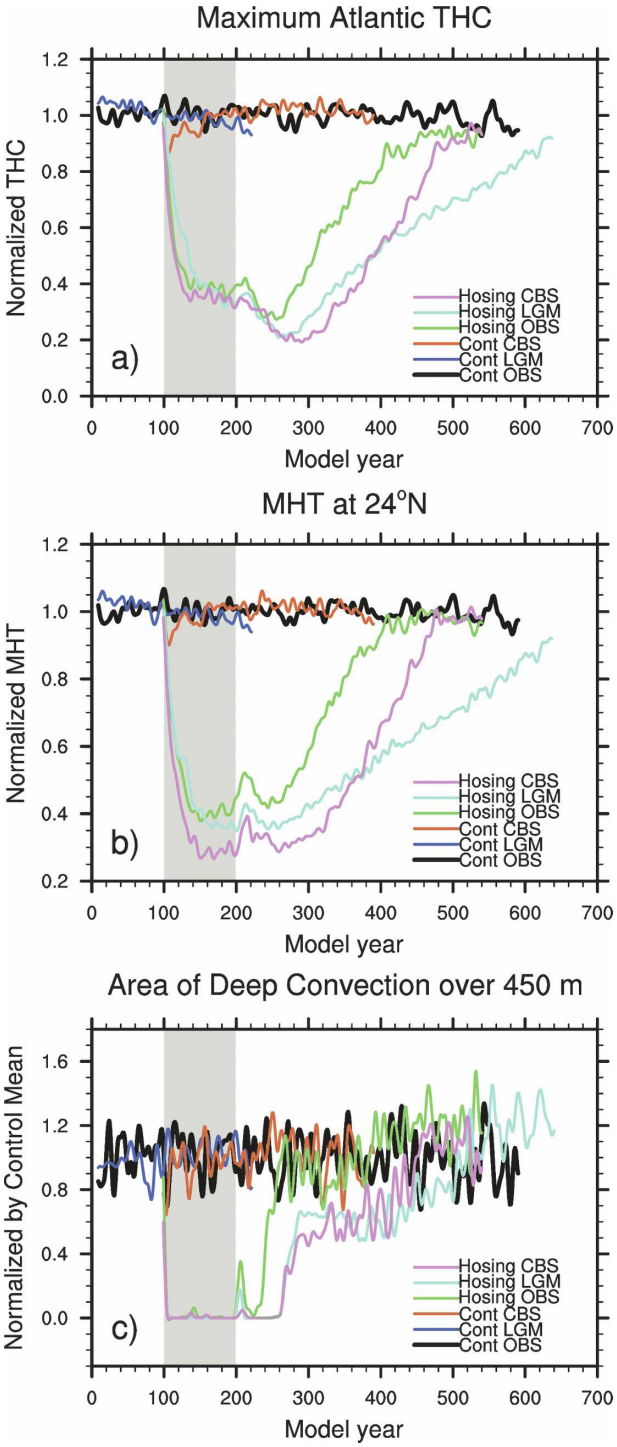

FIG. 1. (a) The 13-yr low-pass-filtered maximum Atlantic THC index, (b) the Atlantic meridional heat transport at 24°N, and (c) the March area of deep convection over 450 m deep. All values shown here are normalized by the mean values in the control runs. The mean THC is 15.6, 18.3, and 17 Sv for the OBS, CBS, and LGM control runs, respectively. The mean meridional heat transport at 24°N is 0.85, 0.95, and 1.16 PW (PW $\equiv 10^{15}$ W) for the OBS, CBS, and LGM control runs. The mean March area of deep convection in the North Atlantic is 1.11, 1.50, and 1.65 million square kilometers for the OBS, CBS, and LGM control runs. The shading indicates the 100-yr hosing period.

associated with North Atlantic Deep Water is shallower (Otto-Bliesner et al. 2007) than under present-day conditions (22 Sv; Collins et al. 2006). The shoaling of North Atlantic Deep Water is consistent with the proxy interpretations of Marchitto et al. (2002) and McManus et al. (2004). The paleorecord only cannot determine whether the THC during LGM was stronger or weaker than present day (Yu et al. 1996; McManus et al. 2004). Results from the recent Paleoclimate Modelling Intercomparison Project (PMIP2) suggest that the LGM THC was neither appreciated weaker nor stronger than modern (Weber et al. 2007; Otto-Bliesner et al. 2007).

As shown in Fig. 1a, in all of the hosing experiments the THC decreases dramatically during the first decade after freshwater was added, and then the rate of weakening becomes slower. By the end of the 100-yr hosing, the percentage change of the THC in all three experiments is almost the same. After the termination of the additional freshwater forcing, the THC continuously weakens for some decades before it starts to recover. The recovery of the THC starts 60 yr after the freshwater hosing was terminated in the OBS run, 90 yr in the LGM run, and 100 yr in the CBS run. Except for the delay in the CBS and LGM THC recovery, the rate of the THC recovery is similar between the OBS and CBS hosing runs, but slower in the LGM hosing run than in the OBS hosing run. On the other hand, although the THC begins to recover a decade earlier in the LGM run than in the CBS run, the slower rate of the THC recovery in the LGM hosing run, especially beyond year 400, results in a longer time scale for the THC to return to its control strength after the THC starts to recover in the LGM hosing run. It takes about 350 yr for the THC to return to the strength it had in the control run after the THC starts to recover in the LGM hosing run, but 200 yr in the CBS hosing runs.

Evolution of the meridional heat transport at 24°N in the Atlantic basin mimics that of the THC in all three hosing experiments (Fig. 1b). As THC declines (strengthens), the meridional heat transport also declines (strengthens) with almost the same time scale. This agrees with previous studies that indicate that the meridional heat transport in the Atlantic basin is quasi-linearly correlated to the strength of the THC (Bryan and Holland 1989; Smith et al. 2000; Hu 2001). The decline of the meridional heat transport induces a general cooling in the Northern Hemisphere, with the most significant cooling along the path of the Gulf Stream's northward extension, the North Atlantic Current, agreeing well with previous studies (e.g., Stocker 2002).

The strength of March deep convection measured by the area of the March mixed layer with depths over 450 m is shown in Fig. 1c as time series and in Fig. 2 as

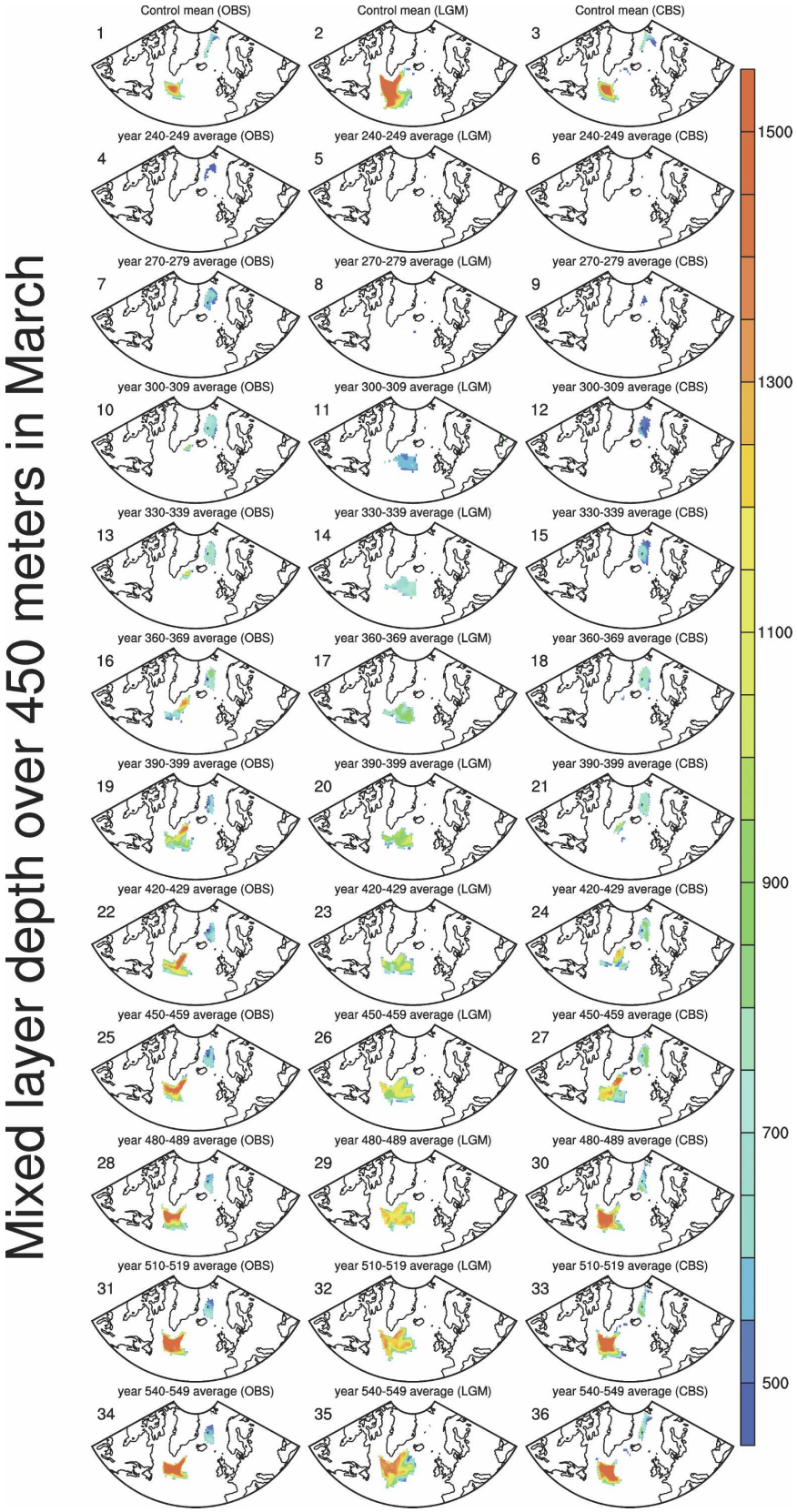

FIG. 2. The mean mixed layer depth in March over 450 m deep. Panels 1–3 are the mean March mixed layer depth in the control runs, and the rest of the panels are the decadal means of the March mixed layer depth in the hosing runs.

decadal mean. As the THC collapses, the deep convection associated with it in the North Atlantic ceases in all three hosing experiments (Fig. 1c). The North Atlantic deep convection starts to reemerge about 40 yr after the termination of the freshwater forcing in the OBS run and 65 yr in the LGM and CBS hosing runs. In the OBS run, the area of deep convection reaches about 90% of its value in the control run in about 20 yr. The area of deep convection jumps to about 65% of that in the control run in about 25 yr for the LGM run, and in about 60 yr in the CBS run, then plateaus for a while before it reaches that in the control runs. However, after the plateau it takes about 50 yr for the area of deep convection to retain the same area as in the control run for the CBS run, but 150 yr for the LGM run. In comparison to Fig. 1a, the recovery of the THC is delayed by more than 20 yr after the reemergence of the deep convection in all three hosing runs, with the longest delay in the CBS run.

The panels 1–3 of Fig. 2 are the mean March mixed layer depth in OBS, LGM, and CBS control runs. These panels show that the deep convection only happens in the North Atlantic between 40° and 65°N in the LGM control simulation, but in both the Nordic seas and the Labrador Sea under present-day conditions. This location of the LGM deep convection is consistent with the suggestions from the paleorecord (Duplessy et al. 1988; Pflaumann et al. 2003) and is associated with the more intensive sea ice coverage in the North Atlantic at that time. Since the deep convection ceases during the hosing in all hosing runs, the decadal mean March mixed layer depth over 450 m shown in Fig. 2 is only for the recovery phase with an interval of 30 yr. In this phase, the convection restarts in the Nordic seas first in both OBS and CBS runs, but south of the Denmark Strait region in the LGM run, as the oceanic stratification weakens due to the divergence of the additional freshwater forcing out of those regions. The timing of this restart is delayed by 30–50 yr in the CBS and LGM runs compared to the OBS run (panels 4–12 in Fig. 2). The comparison between panels 4–36 in Fig. 2 and Figs. 1a,c also suggests that the area of deep convection increases first, then the intensity of the deep convection increases, especially in the area south of 65°N. The initial quick increase in the area of the deep convection indicates a restart of the THC, and the later intensity increase of the deep convection associated to the destabilized oceanic stratification in the subpolar North Atlantic leads to the full recovery of the THC. The deep convection in the Labrador Sea region reaches the same intensity as in the control run in the decade of 450–459 in the OBS run, and in the decade of 480–490 in the CBS run. In the LGM hosing run, the recovery of the deep convection intensity takes longer than in the CBS and OBS runs.

TABLE 2. Bering Strait mass, liquid freshwater, and ice transport. The observed Bering Strait transport is based on Aagaard and Carmack (1989) and Woodgate and Aagaard (2005).

	Mass	Freshwater	Ice
Observations	0.8 Sv	0.053~0.077 Sv	0.003 Sv
OBS control	0.81 Sv	0.062 Sv	0.003 Sv
LGM control	—	—	—
CBS control	—	—	—

b. Freshwater removal from the Atlantic basin

Next, we will discuss the freshwater removal processes in the Atlantic, especially the North Atlantic, and how these removal processes affect the recovery of the THC. Since the CCSM ocean component uses a virtual salt flux instead of the actual freshwater volume flux to represent freshwater exchange between ocean and atmosphere, the oceanic meridional freshwater transport in this paper is calculated as

$$V_{\mathrm{fw}} = \int\int \upsilon(1 - s/s_0)\, dx\, dz\ ,$$

where V_{fw} represents the meridional freshwater transport, υ is the meridional velocity of the ocean, s is the water salinity, and s_0 is the reference salinity that is defined as the global mean salinity (34.7). A positive value of υ is defined as water flowing northward. The value of $\upsilon(1 - s/s_0)$ is integrated zonally (dx) within an ocean basin or strait, and vertically (dz). Equation (1) can be interpreted such that if the water salinity is lower (higher) than the reference salinity, and the water flows northward, the freshwater is transported northward (southward).

1) BERING STRAIT AND ARCTIC

Since H07 and Hu and Meehl (2005a) have pointed out the importance of the freshwater transport from the Arctic into the North Pacific on the THC recovery under present-day conditions using CCSM2, here we review the variation of the Bering Strait Throughflow in the OBS runs first. The volume mass transport at the Bering Strait in the OBS control run is about 0.81 Sv from the Pacific into the Arctic, agreeing well with the observed estimation of 0.8 Sv (Aagaard and Carmack 1989; Woodgate and Aagaard 2005; see Table 2 for a summary). At the same time, about 0.003 Sv of ice is transported into the Arctic through the Bering Strait, comparable to the recent observations (0.003 Sv; Woodgate and Aagaard 2005). The total freshwater transported into the Arctic through the Bering Strait is

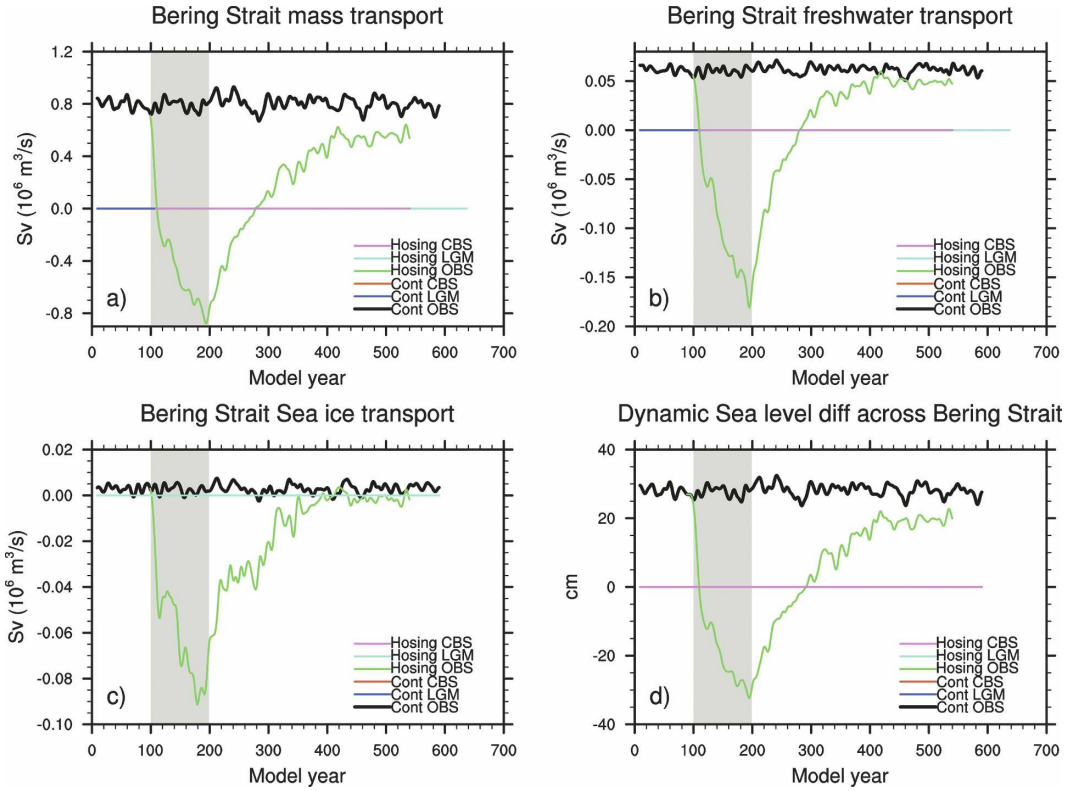

FIG. 3. (a) The 13-yr low-pass-filtered Bering Strait mass, (b) freshwater, (c) ice transports, and (d) the dynamic sea level difference across the Bering Strait from the west side (Alaska side) to the east side (Siberian side). The unit for the transports is Sv and the unit for the dynamic sea level difference is cm. The shading indicates the 100-yr hosing period.

about 0.065 Sv, including 0.062 Sv as liquid freshwater and 0.003 Sv as ice. This total freshwater transport is within the range of the observed values [e.g., 0.053 Sv by Aagaard and Carmack (1989) and 0.08 Sv by Woodgate and Aagaard (2005)]. In the OBS hosing run, the direction of the Bering Strait transports, including mass, freshwater, and sea ice, reverses from a transport of the Pacific water into the Arctic to a transport of the Arctic water into the Pacific at year 110, a decade after the start of the hosing as the THC weakens (Figs. 3a–c). Then, 170 yr later, the direction of the Bering Strait transports changes back to the direction as in the control run. During this 170-yr period with a reversed Bering Strait transport, an equivalent of 23% of the total freshwater (hereafter, Q_{fwaddtot}) added into the subpolar North Atlantic during that 100-yr hosing period is directly transported into the Pacific at the Bering Strait. If the anomalous freshwater transport in the OBS hosing run relative to the control run is considered, the freshwater gain in the North Pacific is equivalent to about 22% of the Q_{fwaddtot} during that 100-yr hosing period, and increases to 37% 100 yr after the termination of the additional freshwater flux. It is about 43% for the whole duration of the OBS hosing experiment (H07; see Table 3 and Fig. 4 for a summary). Since the Bering Strait is closed, this important freshwater transport process is absent in the CBS and the LGM runs.

As discussed by Hu and Meehl (2005a) and H07, in

TABLE 3. Liquid freshwater and ice transport at the Bering Strait in the OBS hosing experiment. The cumulative transport of anomalous liquid water and ice relative to the OBS control run shown in this table are normalized by the total freshwater added into the subpolar North Atlantic (Q_{fwaddtot}). The numbers shown here are the percentage of the Q_{fwaddtot}. Negative numbers indicate the freshwater is transported southward from the Arctic into the Pacific.

	100–199	200–299	300–399	400–499	500–549	100–549
Liquid freshwater	−15.4	−10.8	−2.5	−1.2	−0.7	−30.6
Ice	−6.3	−4.1	−1.1	−0.3	−0.3	−12.1

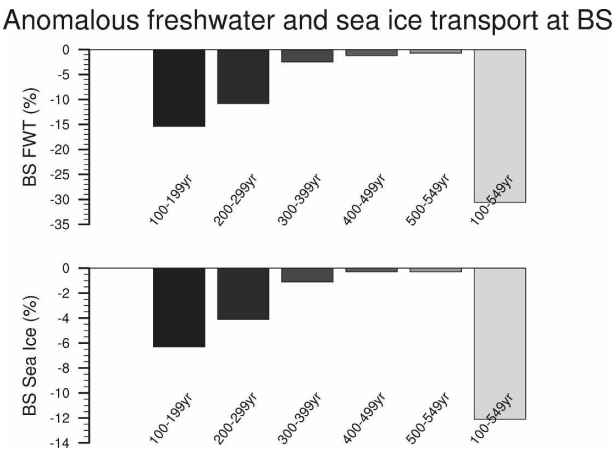

FIG. 4. Freshwater and sea ice transport anomaly at the Bering Strait in the OBS hosing run. The negative values indicate a southward transport—from the Arctic to the North Pacific. Each of the bars represents the percentage of the total freshwater anomaly added into the subpolar North Atlantic being transported out of the Atlantic via the Bering Strait during the period indicated in the figure.

the OBS control run about 4 Sv of Southern Ocean water is pushed into the Atlantic by Southern Ocean winds agreeing with De Boer and Nof (2004a,b). In the OBS hosing run, since the THC does not completely cease, only about 1 Sv of upper-ocean water forced into the Atlantic at 30°S by winds flows into the Pacific at the Bering Strait in the last decade of the hosing. The rest of that water still returns to the Southern Oceans via the lower limb of the THC. Thus, in our OBS simulation less freshwater is pushed into the Pacific via the Bering Strait resulting in a much longer recovery time for the THC in the OBS simulation than in De Boer and Nof's studies.

Another explanation regarding the Bering Strait flow reversal is revealed by studies of Overland and Roach (1987) and Shaffer and Bendtsen (1994), who have shown that the Bering Strait Throughflow is primarily controlled by the dynamic sea level difference between the Pacific and the Arctic. In the OBS control run, the mean dynamic sea level in the North Pacific (40°–60°N) is higher than that in the Arctic with a northward flow of 0.81 Sv. Because of the earth's rotation, this northward flow at the Bering Strait results in a sea level difference across the Bering Strait from west (Alaska side) to east (Siberian side). As shown in Fig. 5, this sea level difference at Bering Strait is nicely correlated with the Bering Strait mass transport in both of the OBS control run and the hosing run. In the OBS hosing run, the time evolution of this sea level difference indicates that the reversal of the Bering Strait Throughflow is

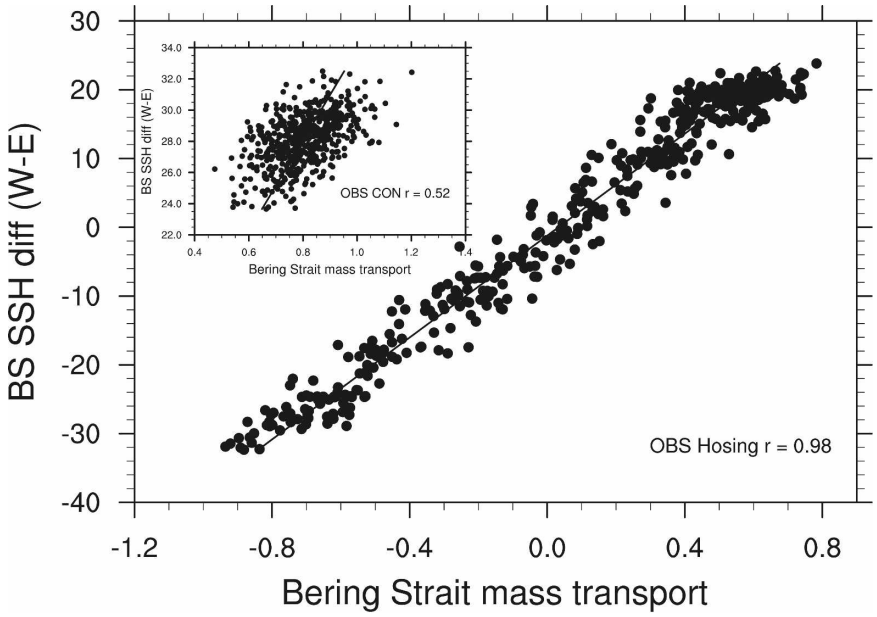

FIG. 5. Scatterplot of the sea level difference across Bering Strait from west (Alaska side) to east (Siberian side) and the Bering Strait mass transport in the OBS control and hosing runs. The figures show that the Bering Strait mass transport is highly correlated by the sea level difference across the Bering Strait. When the sea level difference changes sign, the Bering Strait mass transport reverses the flow direction. This indicates that the mass transport at Bering Strait is primarily controlled by the sea level difference between the North Pacific and the Arctic.

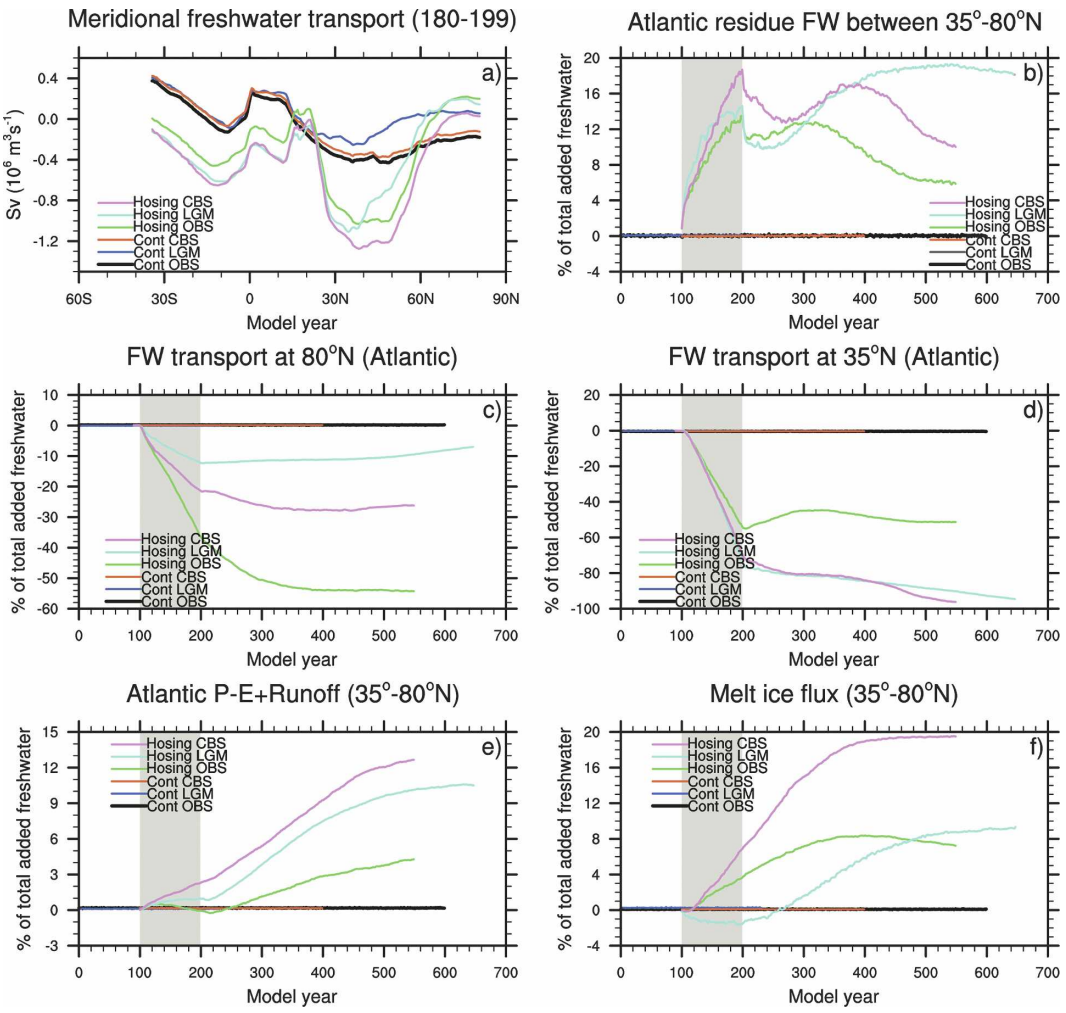

FIG. 6. (a) The mean meridional freshwater transport in the Atlantic in the control runs and the meridional freshwater transport averaged over the last 20 hosing years for the hosing runs. (b) The 13-yr low-pass-filtered cumulative residue freshwater anomaly in the Atlantic between 35° and 80°N; the cumulative freshwater transport at (c) 80°N and (d) 35°N; (e) the cumulative surface freshwater input anomaly from precipitation, evaporation, and river runoff ($P - E + R$) in the Atlantic between 35° and 80°N; and (f) the cumulative melting ice flux anomaly in this region. In (b)–(f), positive (negative) values represent a freshwater loss (gain) by the ocean. All values in (b)–(f) are normalized by the total additional freshwater added into the subpolar North Atlantic during the 100-yr hosing period (Q_{fwaddtot}). The latitude of 80°N is defined as along the line of 80°N latitude from 90°W to 30°E and along the line of 30°E from 80° to 70°N.

consistent with the reversal of the pressure gradient between the North Pacific and the Arctic in the OBS hosing run (Figs. 3a,d).

2) CHANGES IN MEAN OCEANIC MERIDIONAL FRESHWATER TRANSPORT

Figures 6a and 7 are the mean meridional freshwater transport in the Atlantic basin. The three curves for the OBS, CBS, and LGM control runs (black, red, and blue lines, respectively) in Fig. 6a show roughly similar strengths of the meridional freshwater transport in the South Atlantic, though with slightly higher northward transport values in the CBS and LGM runs, which might be associated with the changes of the Southern Ocean winds in these two cases relative to the OBS case. In the North Atlantic, the southward freshwater transport is smaller in the LGM run than in the OBS and CBS runs. At 80°N (defined as along the line of 80°N latitude from 90°W to 30°E and along the line of 30°E from 80° to 70°N) freshwater is transported from the Arctic into the North Atlantic in the OBS and CBS control runs, but from the North Atlantic into the Arc-

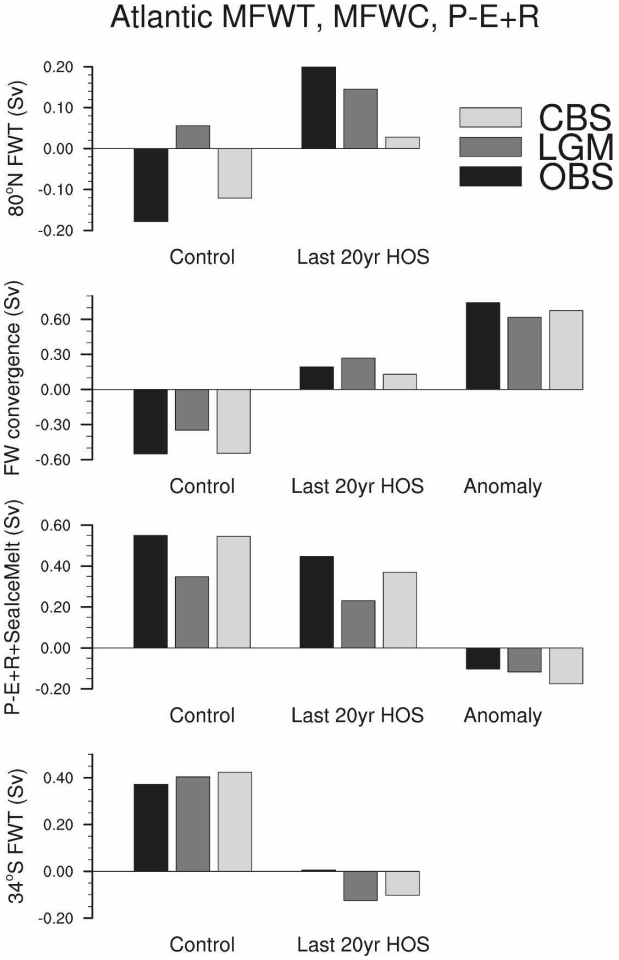

FIG. 7. The meridional freshwater transport at (top) 80°N and (bottom) 34°S; (third from top) the surface freshwater input from precipitation, evaporation, river runoff ($P - E + R$), and the melting sea ice; and (second from top) the meridional freshwater divergence for the control and hosing runs of the OBS (dark bars), LGM (lighter bars), and CBS (light bars) cases. The unit is Sv. The latitude of 80°N is defined as along the line of 80°N latitude from 90°W to 30°E and along the line of 30°E from 80° to 70°N. The positive (negative) values represent a northward (southward) meridional freshwater transport. Positive values of the $P - E + R$ and sea ice melting indicate a freshwater loss. The positive (negative) values of the meridional freshwater divergence represent a freshwater loss (gain).

tic in the LGM control run. In the OBS control run, the Arctic accepts similar amount of freshwater as the observed from the Pacific via the Bering Strait, and from precipitation, evaporation, and river runoff ($P - E + R$), then exports this freshwater gain into the North Atlantic (Fig. 7 and Table 4). Since the Bering Strait is closed in both CBS and LGM control runs, there is no freshwater flowing from the Pacific into the Arctic. However, in the CBS control run, the Arctic gains freshwater because of $P - E + R$, and subsequently this freshwater is transported into the North Atlantic. In the LGM condition, the Arctic loses a small amount of freshwater primarily by sea ice export. To balance this loss in the Arctic in the LGM control run, freshwater has to be imported into the Arctic from the North Atlantic via ocean transport (Fig. 7 and Table 4).

By the end of the hosing, the meridional freshwater transport is similar throughout the Atlantic basin in these three runs. Noticeably, the freshwater transport at 80°N reverses direction in both OBS and CBS hosing runs from an import of freshwater into the Atlantic basin to an export of freshwater into the Arctic (see Fig. 7 and Table 4 for a summary). In the LGM hosing run, the export of freshwater from the Atlantic into the Arctic is more than double of that in the LGM control run. At the southern end of the Atlantic basin, the freshwater transport changes from an import from the Southern Ocean to an export from the Atlantic into the Southern Oceans in the LGM and CBS hosing runs, and is significantly reduced in the OBS hosing run (Fig. 7 and Table 4). These changes lead to a net freshwater divergence in the Atlantic basin due to oceanic meridional freshwater transport in all three hosing runs in contrast to the control runs. Overall, the rate of the freshwater removal is faster in the OBS hosing run than in the LGM and CBS runs. As shown in Fig. 7 and Table 4, the oceanic freshwater removal process is almost equally important at the southern and northern ends of the Atlantic Ocean in the OBS hosing run, but is dominated by transport at the southern end in the LGM and CBS run.

3) TIME-EVOLVED FRESHWATER REMOVAL IN THE ATLANTIC (35°–80°N)

How this faster freshwater removal in the Atlantic basin would affect the recovery of the THC and the associated deep convection in the North Atlantic marginal seas can be addressed through an analysis of the freshwater budget in the Atlantic. Since the deep convection in the LGM runs is located at south of the 65°N and extends to about 35°N, the area of this freshwater budget analysis is from 80° to 35°N in the Atlantic, a bit different from H07 who used 40°N as the southern boundary of their freshwater budget analysis. The freshwater removal from the North Atlantic basin between 35° and 80°N to other ocean basins due to oceanic and atmospheric processes is shown in Figs. 6b–f and summarized in Fig. 8 and Table 5.

The freshwater anomaly in this region is defined as the residue of the surface freshwater flux and the oceanic freshwater divergence in the hosing runs relative to their control runs, with the value shown in Fig. 6b the percentage of the total additional freshwater added into

TABLE 4. Meridional oceanic freshwater transport at 80°N and 34°S. The meridional freshwater transport shown in this table is the mean for the control runs and a mean averaged over the last 20 yr of hosing for the hosing runs (Hos_last20yr). The unit is Sv. 80°N and 34°S indicate the rate of freshwater transport at these latitudes in both control runs and the freshwater hosing runs, and the 80°NA and 34°SA represent the freshwater transport anomaly in the freshwater hosing runs relative to their control run. MFWD represents the meridional freshwater divergence and MFWDA is the meridional freshwater divergence anomaly in the hosing runs relative to their control runs. Positive (negative) values indicate a northward (southward) meridional freshwater transport or a freshwater divergence (convergence) in the Atlantic basin. The latitude of 80°N is defined as along the line of 80°N latitude from 90°W to 30°E and along the line of 30°E from 80° to 70°N.

	OBS		LGM		CBS	
	Control	Hos_last20yr	Control	Hos_last20yr	Control	Hos_last20yr
80°N	−0.178	0.199	0.056	0.145	−0.121	0.028
80°NA	—	0.377	—	0.089	—	0.149
34°S	0.372	0.006	0.404	−0.124	0.424	−0.102
34°SA	—	−0.366	—	−0.528	—	−0.526
MFWD	−0.550	0.193	−0.348	0.269	−0.545	0.130
MFWDA	—	0.743	—	0.617	—	0.675

this region in the 100-yr hosing period (Q_{fwtotadd}). During the hosing the residue freshwater anomaly increases with time, indicating that there is a net freshwater gain in this region owing to the inability of the climate system to transport all of the anomalous freshwater added into this region out to other ocean basins. By the end of the hosing, the residue freshwater anomaly is highest in the CBS run and lowest in the OBS run (Fig. 8 and Table 5). After the hosing, the freshwater anomaly follows a pattern of decrease, increase, and decrease again in all three runs. In a comparison of Figs. 1a and 6b, the start of THC recovery almost coincides with the in-

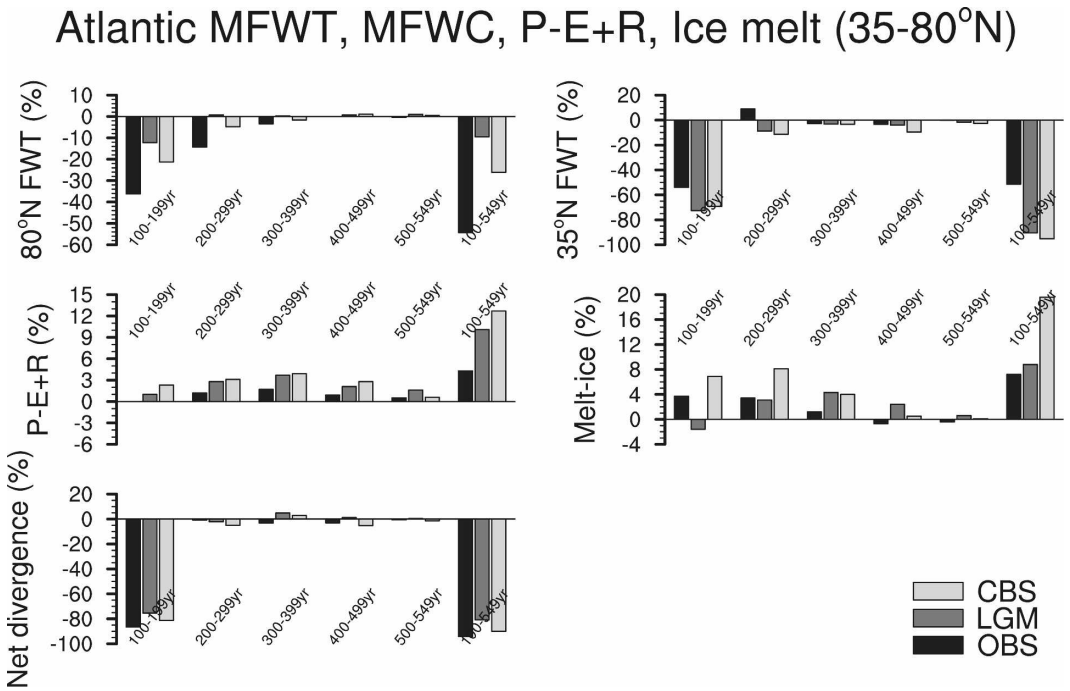

FIG. 8. The anomalous meridional freshwater transport at 80°N, 35°N; the surface freshwater input anomaly from precipitation, evaporation, and river runoff ($P - E + R$); the melt–ice flux anomaly; and the net freshwater divergence in the region of the North Atlantic between 35° and 80°N in the three hosing runs. Values shown in these figures are the percentage of the total freshwater anomaly added into the subpolar North Atlantic during the 100-yr hosing period. The bars show the anomalous freshwater transport (or input) in the given period in the figures. Bars from darker to lighter color represent the OBS, LGM, and CBS cases, respectively. Negative (positive) values are freshwater being transported out (added into) the Atlantic between 35° and 80°N.

TABLE 5. Freshwater (FW) budget analysis in the Atlantic between 35° and 80°N. Numbers shown in this table are the percentage of the total additional freshwater added into the subpolar North Atlantic (Q_{fwaddtot}). The positive (negative) values indicate a freshwater gain (loss) to the Atlantic region between 35° and 80°N. The residue freshwater anomaly is the percentage value of the total additional freshwater input into the North Atlantic during the 100-yr hosing period, which still stays in the North Atlantic between 35° and 80°N by the end of the year indicated in the table. The latitude of 80°N is defined as along the line of 80°N latitude from 90°W to 30°E and along the line of 30°E from 80° to 70°N.

		100–199	200–299	300–399	400–499	500–549	100–549
FW transport 80°N	OBS	−36.2	−14.3	−3.4	0.0	−0.4	−54.3
	LGM	−12.2	0.7	0.3	0.7	1.0	−9.5
	CBS	−21.3	−4.8	−1.6	1.1	0.5	−26.1
FW transport 35°N	OBS	−53.9	8.9	−2.8	−3.4	−0.2	−51.4
	LGM	−72.6	−8.8	−3.2	−4.0	−1.7	−90.3
	CBS	−69.2	−11.4	−3.4	−9.6	−2.6	−96.2
Oceanic FW divergence	OBS	−90.1	−5.4	−6.2	−3.4	−0.6	−105.7
	LGM	−84.8	−8.1	−2.9	−3.3	−0.7	−99.9
	CBS	−90.5	−16.2	−5.0	−8.5	−2.1	−121.3
$P - E + R$	OBS	−0.0	1.2	1.7	0.9	0.5	4.3
	LGM	1.0	2.8	3.7	2.1	1.6	10.1
	CBS	2.3	3.1	3.9	2.8	0.6	12.7
Melt–ice	OBS	3.7	3.4	1.2	−0.6	−0.4	7.2
	LGM	−1.6	3.1	4.3	2.4	0.6	8.8
	CBS	6.9	8.1	4.0	0.5	0.1	19.6
Net FW divergence	OBS	−86.5	−0.8	−3.2	−3.1	−0.5	−94.1
	LGM	−85.4	−2.1	4.9	1.2	0.4	−80.8
	CBS	−81.3	−5.0	2.9	−5.2	−1.4	−90.0
		Yr 199	Yr 299	Yr 399	Yr 499	Yr 549	
Residue FW	OBS	13.5	12.7	9.5	6.4	5.9	
	LGM	14.6	12.5	17.6	18.8	19.2	
	CBS	18.7	13.7	16.6	11.4	10.0	

crease of the residue freshwater anomaly. Since the strengthening of the THC after the hosing will strengthen the northward flow in the upper ocean, part of the freshwater—exported from the subpolar hosing zone southward into the subtropical, tropical, and South Atlantic previously—is transported back into the subpolar North Atlantic by this northward flow of the THC upper limb. This increase of freshwater anomaly is largest and lasts longest in the LGM hosing run, and smallest and shortest in the OBS hosing run, and is one reason for a slower acceleration of the THC in the LGM hosing run after the switch off of the freshwater forcing. As the THC recovers, the lower limb of the THC starts to export the freshwater anomaly southward, and the upper limb transports saltier water northward, leading to a subsequent decrease of the residue freshwater anomaly in the hosing runs.

The contribution of each of the four freshwater terms—the oceanic freshwater transport at 80° and 35°N, the $P - E + R$, and the melt sea ice water—to the freshwater removal process and the recovery of the THC are shown in Figs. 6c–f and 8. At 80°N there is more freshwater flowing northward into the Arctic in the OBS hosing run than in the CBS and LGM hosing runs (Fig. 6c). In comparison to the corresponding control runs, the freshwater anomaly transported into the Arctic as liquid water in the OBS hosing run at the end of the hosing is 50% higher than in the CBS run and is about 2 times greater than that in the LGM run (Fig. 8 and Table 5). In addition to the effect of the Bering Strait, the much lower freshwater gain in the Arctic in the LGM run is caused by the more extensive sea ice coverage. The Nordic seas are almost fully covered by sea ice in the LGM control, especially in winter months (Otto-Bliesner et al. 2006), and are fully covered by sea ice over a meter thick in the LGM hosing runs. This rigid ice cover reduces the momentum transfer from the air to the ocean. Thus, the resulting oceanic flows between the North Atlantic and the Arctic are much weaker in the LGM runs than in the OBS and CBS runs, leading to less freshwater being exported into the Arctic from the subpolar North Atlantic in the LGM hosing run. In addition, the lower sea level in the LGM conditions closes the oceanic pathway between the Nordic seas and the Arctic through the Barents Sea. The only connection between the Nordic seas and the Arctic is the narrower pathway of the Fram Strait. This results in a reduced water mass exchange between the Arctic and the Nordic seas (also the North Atlantic). After the hosing the Arctic continuously gains a significant amount of the anomalous freshwater from the North Atlantic in the OBS run. This continued north-

ward freshwater transport at 80°N is associated with the freshwater export through the Bering Strait. On the other hand the liquid freshwater starts to be exported from the Arctic into the North Atlantic roughly two centuries after the end of the hosing in the CBS hosing run and right after the end of the hosing in the LGM run, contributing to the elevated freshwater supply after the hosing.

At 35°N the cumulative southward freshwater transport at the end of the hosing is the lowest in the OBS run and highest in the LGM hosing runs, respectively (Figs. 6d and 8 and Table 5). The higher southward freshwater transports in the CBS and LGM hosing runs are associated with the closed Bering Strait. In the first century after the hosing, freshwater is continuously exported southward in the LGM and CBS hosing runs, but imported into the subpolar North Atlantic in the OBS run owing to the early start of the THC recovery discussed earlier. Overall, more than 90% of the freshwater added in the subpolar North Atlantic is transported southward at 35°N in the CBS and LGM hosing runs during the 450-yr period, but only 51% of $Q_{fwaddtot}$ in the OBS run. This further confirms that a closed Bering Strait forces the additional freshwater to be transported southward in the CBS and LGM hosing runs.

The surface freshwater input anomaly due to $P - E + R$ varies similarly in these three hosing simulations (Figs. 6e and 8). In the OBS hosing run, the changes of the surface freshwater input anomaly due to $P - E + R$ is small during the hosing and the 60-yr period right after the hosing. Then this anomaly increases with time and reaches about 4% of $Q_{fwaddtot}$ at the end of the integration. In the CBS and LGM hosing runs, this anomaly increases with time during the whole period of integration. Although precipitation, evaporation, and river runoff into this region decrease because of the cooler climate induced by the weakened THC, the reduction of the evaporation is much larger than the reduction of the precipitation and river runoff, leading to an increased freshwater supply in all hosing runs compared to the control runs, especially in the CBS and LGM hosing runs. Overall, the cumulative surface freshwater input is much higher in the LGM and CBS hosing runs than in the OBS hosing run, contributing to the delayed recovery of the THC in the LGM and CBS hosing runs.

The freshwater input anomaly from melting sea ice increases over time in the CBS hosing run, with a cumulative contribution up to 20% of $Q_{fwaddtot}$ (Figs. 6f and 8), leading to a delayed recovery of the THC. As indicated by H07, this increased freshwater input due to sea ice melting is associated with the export of the freshwater as sea ice from the Arctic into the North Atlantic region. This exported freshwater comes from the freshwater imported from the subpolar North Atlantic into the Arctic during the hosing and some years after the hosing. In the OBS hosing run, the melting sea ice water also increases over time, but at a much slower rate. The supply of this meltwater starts to decline about 150 yr after the hosing. The overall contribution of this melting sea ice water to the surface freshwater anomaly is about 7% of $Q_{fwaddtot}$. In the LGM hosing run, the anomaly of the melt sea ice water decreases during the hosing, indicating that the further chilling effect due to the weakened THC is so strong it prevents a net sea ice melting in this region (or it produces a net sea ice production in this region). This process contributes to the lower freshwater anomaly by the end of hosing and the earlier acceleration of the THC after the hosing in the LGM hosing relative to the CBS hosing run. An increased melt sea ice water relative to the control run occurs only after the end of the hosing with a cumulative contribution to the surface freshwater input anomaly up to 9% of the $Q_{fwaddtot}$. The cumulative surface freshwater input anomalies due to both $P - E + R$ and melting ice are much higher in the CBS and LGM hosing runs than in the OBS hosing run over 450-yr period (Fig. 8 and Table 5).

In summary, the divergence of the freshwater anomaly is dominated by the southward freshwater transport at 35°N in the CBS and LGM hosing runs. In the OBS hosing run, the southward (at 35°N) and northward (at 80°N) freshwater transports are equally important to the divergence of the freshwater anomaly because of the export of the freshwater anomaly to the Pacific via the Bering Strait. The changes of the surface freshwater anomaly from $P - E + R$ and melt sea ice are similar in all three hosing runs, but the total surface freshwater input anomalies are higher in the CBS and LGM hosing runs than in the OBS hosing run, leading to a slower acceleration of the THC after the hosing. Although the relative contributions of each of the freshwater terms are a bit different, the overall effects of these terms on THC are similar in the CBS and LGM hosing runs but different in the OBS hosing run, especially the oceanic freshwater divergences that are the dominant term for the freshwater removal from the subpolar North Atlantic region in all of the experiments. Although a certain amount of the added freshwater flows into the Arctic during the hosing, this water is exported back to the subpolar North Atlantic as sea ice and liquid water after the hosing in the CBS and LGM hosing runs, leading to an elevated freshwater supply in the subpolar North Atlantic and thus delaying the recovery of the THC. On the other hand, this water

flowing into the Arctic from the subpolar North Atlantic is mostly exported into the Pacific through the open Bering Strait in the OBS run. Therefore, the importance of the closed Bering Strait on oceanic freshwater divergence in the Atlantic between 35° and 80°N and the THC recovery is similar in the CBS and LGM hosing runs.

4) Interbasin salinity contrast, meridional steric height gradient, and THC

Locally, it is important to remove the anomalous freshwater from the subpolar North Atlantic in order to get the deep convection in the region reactivated and initiate the recovery of the THC. However, the remote effects seem also important in controlling the recovery processes of the THC after the end of the hosing (e.g., Hu et al. 2004, and their references). One of the remote factors controlling the THC strength is the sea surface salinity (SSS) contrast between the North Atlantic and the North Pacific between 10° and 60°N (Seidov and Haupt 2003, 2005), which represents the efficiency of the freshwater transport from the Atlantic to Pacific via atmospheric circulation. A stronger SSS contrast between these two basins is related to a stronger THC, and vice versa, for the equilibrium state (Seidov and Haupt 2003, 2005) and the century–time scale transient climate state (Hu et al. 2004) as long as the changes of the THC are primarily caused by freshwater anomalies. In all the hosing experiments, as freshwater is added into the North Atlantic the SSS difference between North Atlantic and North Pacific decreases, agreeing with the changes of the THC (left panels in Fig. 9). In the OBS hosing run, since part of the additional freshwater flux is transported into the Pacific via the open Bering Strait, which lowers the SSS there, the drop of the SSS contrast is smaller during the hosing, and the recovery of this SSS contrast is quicker after the hosing in comparison with the CBS and LGM hosing runs. Thus, the more rapid recovery of the THC in the OBS hosing run may be at least partly due to this quicker restoration of the SSS contrast between North Atlantic and North Pacific.

The other important factor that may affect the THC strength is the meridional steric height gradient between 60°N and 30°S in the Atlantic, where the steric height anomaly is defined as the zonal and vertical integral of the density anomaly divided by the reference density (1000 kg m^{-3}; Thorpe et al. 2001). Although the exact physics are not clear, studies indicate that this meridional steric height gradient is correlated with the strength of the THC, with a higher gradient associated with a stronger THC in both simple models and fully coupled general circulation models (e.g., Hughes and Weaver 1994; Thorpe et al. 2001; Hu et al. 2004). As freshwater is added in the subpolar North Atlantic, the steric height anomaly decreases significantly at 60°N, leading to a decreased meridional gradient (right panels in Fig. 9) and a weakened THC in all three hosing runs. In the OBS hosing run, because of the quicker removal of the added freshwater in the subpolar North Atlantic, the steric height anomaly at 60°N recovers faster than in the LGM and CBS hosing runs, leading to a quicker restoration of the meridional steric height gradient.

The SSS contrast between North Atlantic and North Pacific correlates well with the THC in both control and hosing runs in the CBS and LGM cases, but only in the hosing run in the OBS case. This may indicate that since this indicator is derived from equilibrium solutions of a coarse resolution model with a closed Bering Strait, it may not be relevant for the THC variations in models with an open Bering Strait if freshwater forcing is not the dominant cause for the THC variation (Hu et al. 2004; Hu and Meehl 2005b; Hu et al. 2007b). The meridional steric height gradient as a proxy for THC variations works well in all three control and hosing runs, agreeing with Hu et al. (2004). This suggests that some mechanisms associated with THC variability in simple models with a closed Bering Strait may not be applicable to modern climate, but may work well for glacial periods when the Bering Strait was closed. Thus we should be cautious when these mechanisms are used to explain modern climate variations.

4. Conclusions and discussion

In this study we successfully extended the conclusion reached by H07 for present-day conditions to the conditions of the last glacial maximum (LGM). We analyzed the response of the THC in three freshwater hosing experiments using the NCAR CCSM2 and CCSM3 with 1 Sv additional freshwater added uniformly into the subpolar North Atlantic between 50° and 70°N for a period of 100 yr. Two of the experiments are under present-day conditions, but one with an open Bering Strait (OBS) and the other one with a closed Bering Strait (CBS). The third hosing experiment is under the LGM conditions with a closed Bering Strait.

Results from these experiments show that a closed Bering Strait induces a delayed recovery of the THC after the additional freshwater flux was turned off in both the present-day and LGM simulations, and an open Bering Strait accelerates the recovery of the THC in the present-day simulation. A freshwater budget analysis in the Atlantic finds that the removal of the additional freshwater added into the subpolar North Atlantic is only achieved by oceanic transport in all

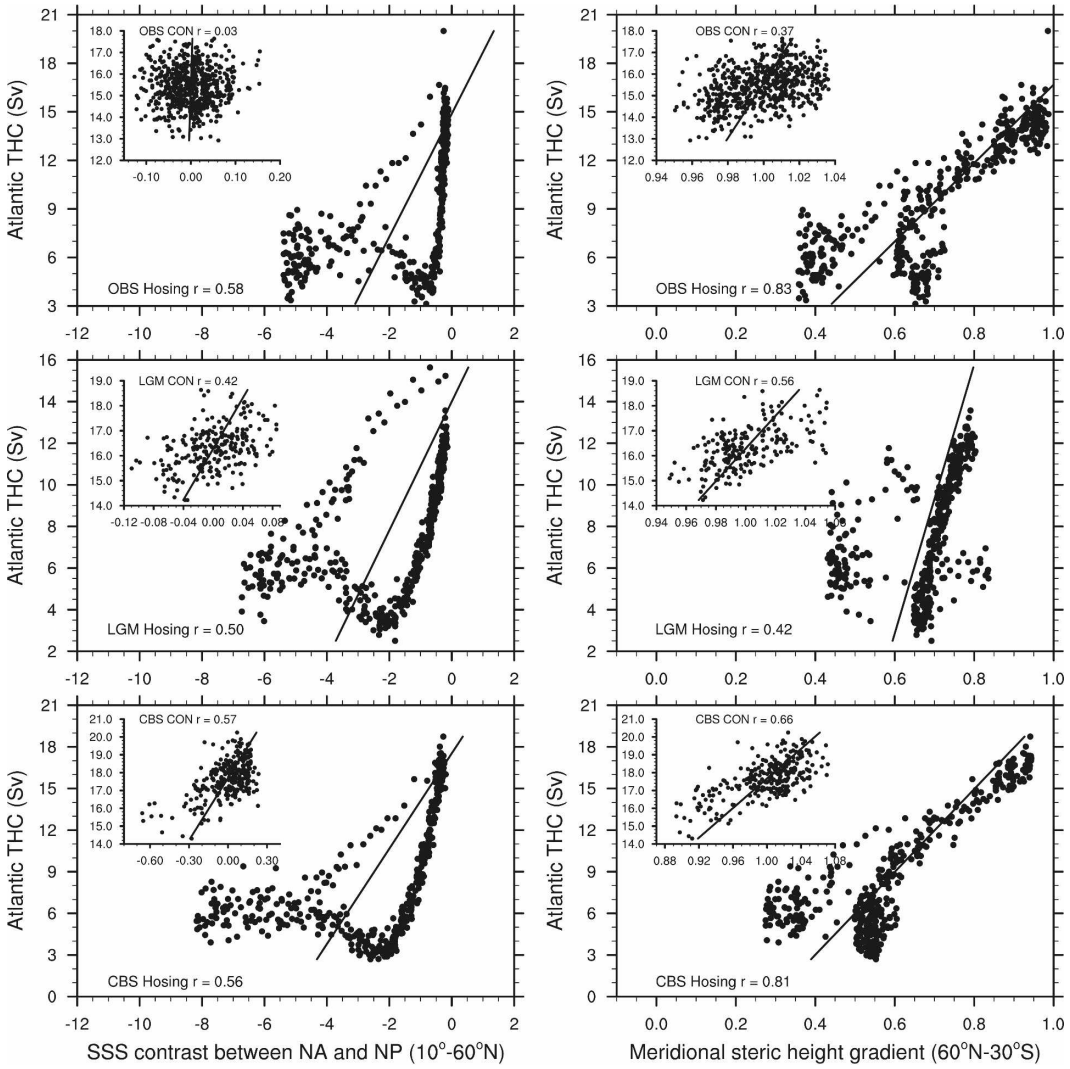

FIG. 9. (left column) The scatterplot of the anomalies of the SSS contrast between the North Atlantic and the North Pacific between 10° and 60°N relative to their control means and the THC indices in the control and hosing runs of all three cases. The mean SSS contrast is 0.70, 1.26, and 1.63 for the OBS, CBS, and LGM control runs, respectively. (right column) The scatterplot of the meridional steric height gradient normalized by their control means and the THC indices. The mean meridional steric height gradient is 1.15, 1.32, 1.15 cm $(\text{deg\_lat})^{-1}$ (centimeter per degree latitude) for the OBS, CBS, and LGM control runs, respectively. The straight lines are the regression lines. The top panels are for the OBS case, the middle panels are for the LGM case, and the bottom panels are for the CBS case.

hosing runs since the net freshwater supply at the surface due to precipitation, evaporation, river runoff, and melting sea ice in the subpolar North Atlantic is higher than that in the control runs throughout these experiments. This freshwater removal is faster in the OBS hosing experiment than in the CBS and LGM runs because the freshwater anomaly is diverged equally southward at 35°N and northward into the Arctic. Most of the freshwater transported into the Arctic is further exported into the North Pacific via the open Bering Strait, which accelerates the removal of the freshwater anomaly from the subpolar North Atlantic. However, in the CBS and LGM hosing runs, freshwater can only be transported southward because of a closed Bering Strait. Although freshwater is also transported into the Arctic during hosing in these two runs, it is transported back into the subpolar North Atlantic after the hosing, mostly as sea ice. Combined with the increased $P - E + R$, the total surface freshwater anomaly is much higher after the hosing in the CBS and LGM hosing runs than in the OBS run, leading to a more stably stratified upper ocean and a delayed recovery of the THC.

Our study suggests that, although other factors or processes may also contribute to the THC variations, the open Bering Strait plays a crucial role in stabilizing the THC on a multicentury time scale because of its ability to transport freshwater in both directions—from the Pacific to the Atlantic under active THC conditions, and from the Atlantic to the Pacific under a condition of the THC shutdown (or near shutdown). In the other words, the Pacific acts as a freshwater reservoir to the subpolar North Atlantic and the Arctic with an open Bering Strait, and the Bering Strait acts as a floodgate. When THC is stronger, more freshwater flows from the North Pacific via the Bering Strait into the North Atlantic, which strengthens the upper-ocean stratification in the latter, and thus weakens the THC. If the THC is too weak, freshwater is removed from the North Atlantic into the North Pacific by a reversed flow through the Bering Strait, resulting in an increased SSS and destabilized upper-ocean stratification in the North Atlantic, and inducing a strengthening of the THC.

This finding could have significant application in both paleoclimate and modern climate studies. The Bering Strait was closed during a significant portion of the last glacial period. The abrupt climate change events, for example, D–O events, Heinrich events, and the Younger Dryas, happened during this period. Since these abrupt climate change events possibly are associated with land glacier discharge, the closed Bering Strait might have provided an environment that favored the occurrence of these events. As shown in this study, the closed Bering Strait prevents a fast removal of the freshwater anomaly in the subpolar North Atlantic, thus strengthening the surface stratification and inducing a slow recovery of the THC after a major shutdown. In the future, as atmospheric CO_2 concentration increases, most of the Intergovernmental Panel on Climate Change Fourth Assessment Report (IPCC AR4) models predict a weakened THC in the twenty-first century, not a collapsed one (Meehl et al. 2007). Results from the NCAR's CCSM3 show that as the THC weakens in the twenty-first century, the mass transport at the Bering Strait decreases. The freshwater transport by this throughflow may not immediately produce a net reduction of the freshwater transport from the Pacific into the Arctic, and further to the Atlantic (because of the melting of the Pacific sea ice and increased precipitation there). However, if the Bering Strait Throughflow does not weaken, more freshwater would be transported into the Arctic and the North Atlantic, leading to a further weakening of the THC. Although the changes of the Bering Strait Throughflow may only be a response (not a control) of the changes of the THC and associated sea level changes in the Atlantic, Arctic, and the Pacific, the net effect of the open Bering Strait is to stabilize the THC on a multicentury time scale. Given the importance of the Bering Strait, it is essential to use the correct Bering Strait condition to study the modern climate and paleoclimate.

It is worth mentioning that the off mode of the THC is not stable in any of our three hosing experiments on a multicentury time scale. Similar results are found for models performing the CMIP or PMIP hosing experiments (Stouffer et al. 2006; C. Morrill et al. 2007, unpublished manuscript). This may suggest that the hysteresis behavior of the THC found in idealized models under very slow freshwater forcing (e.g., Stommel 1961; Bryan 1986; Weaver and Hughes 1992; Stocker and Wright 1991; Mikolajewicz and Maier-Reimer 1994; Rahmstorf 1995) may not exist in the coupled climate models under a strong and fast freshwater forcing, such as 1 Sv additional freshwater forcing for a 100-yr period. In these models, the off mode of the THC may be an advectively unstable mode as suggested by Krebs and Timmermann (2007).

In this study we concentrated on the effect of the freshwater divergence from the hosing zone on the recovery of the THC after the termination of the added freshwater flux into the subpolar North Atlantic Ocean. The different rate of the THC recovery between the CBS and LGM hosing runs suggests that other factors may also play a role in influencing the rate of the THC recovery in the LGM condition, such as sea ice (Bitz et al. 2007; C. Morrill et al. 2007, unpublished manuscript) and forcing from the tropical Atlantic (Krebs and Timmermann 2007). These mechanisms also need to be examined, but are beyond the scope of this paper. The other question that could also be raised is whether our conclusions in this study could be extended to other models, such as the models participating in the coordinated hosing experiments of the Coupled Model Intercomparison Project (Stouffer et al. 2006). A preliminary investigation indicates that the THC and Bering Strait transport in the freshwater hosing experiment in those atmosphere–ocean coupled general circulation models with an open Bering Strait behave similarly to what we have seen in CCSM2. Further study of this question is actively being pursued by the authors but is beyond the scope of the present paper.

There is a small trend of the THC in the LGM control run. It is not clear whether this trend would continue since the LGM control run was not integrated beyond what have shown here. From the comparison of the THC response in the CBS and LGM hosing runs, we speculate that the impact of this trend on the THC's response to freshwater forcing is not large. The conclusion reached in this study would hold, at least qualita-

tively, regardless of any trend in the THC in the LGM control run.

Acknowledgments. We thank Dr. Wei Cheng for many useful discussions on model-produced freshwater transport. We thank Adam Phillips for consulting on the NCL graphics, and Stephanie Shearer and Barbara Ballard for text editing. We thank Drs. Axel Timmermann and Jonathan Gregory, and two anonymous reviewers for their review of this manuscript and their valuable comments. A portion of this study was supported by the Office of Science (BER), U.S. Department of Energy, Cooperative Agreement DE-FC02-97ER62402. Weiqing Han was supported by NSF OCE-0452917 and NASA Ocean Vector Winds Program Award Number 1283568.

REFERENCES

Aagaard, K., and E. C. Carmack, 1989: The role of sea ice and other fresh water in the Arctic circulation. *J. Geophys. Res.,* **94,** 14 485–14 498.

Alley, R. B., and Coauthors, 1993: Abrupt increase in Greenland snow accumulation at the end of the Younger Dryas event. *Nature,* **362,** 527–529.

Bitz, C. M., J. C. H. Chiang, W. Cheng, and J. J. Barsugli, 2007: Rates of thermohaline recovery from freshwater pulses in modern, Last Glacial Maximum, and greenhouse warming climates. *Geophys. Res. Lett.,* **34,** L07708, doi:10.1029/2006GL029237.

Broccoli, A. J., K. A. Dahl, and R. J. Stouffer, 2006: Response of the ITCZ to Northern Hemisphere cooling. *Geophys. Res. Lett.,* **33,** L01702, doi:10.1029/2005GL024546.

Broecker, W. S., 1998: Paleocean circulation during the last deglaciation: A bipolar seesaw? *Paleoceanography,* **13,** 119–121.

Bryan, F. O., 1986: High-latitude salinity effects and interhemispheric thermohaline circulations. *Nature,* **323,** 301–304.

——, and W. R. Holland, 1989: A high resolution simulation of the wind- and thermohaline-driven circulation in the North Atlantic Ocean. *Parameterization of Small-Scale Processes: Proc. 'Aha Huliko'a Hawaiian Winter Workshop,* Honolulu, HI, University of Hawaii at Manoa, 99–115.

Clark, P. U., and A. C. Mix, 2000: Global change: Ice sheets by volume. *Nature,* **406,** 689–690.

——, N. G. Pisias, T. F. Stocker, and A. J. Weaver, 2002: The role of the thermohaline circulation in abrupt climate change. *Nature,* **415,** 863–869.

——, A. M. McCabe, A. C. Mix, and A. J. Weaver, 2004: Rapid rise of sea level 19,000 years ago and its global implications. *Science,* **304,** 1141–1144.

Clarke, G., D. Leverington, J. Teller, and A. Dyke, 2003: Superlakes, megafloods, and abrupt climate change. *Science,* **301,** 922–923.

Collins, W. D., and Coauthors, 2006: The Community Climate System Model Version 3 (CCSM3). *J. Climate,* **19,** 2122–2143.

Dahl, K. A., A. J. Broccoli, and R. J. Stouffer, 2005: Assessing the role of North Atlantic freshwater forcing in millennial scale climate variability: A tropical Atlantic perspective. *Climate Dyn.,* **24,** 325–346.

Dansgaard, W., and Coauthors, 1993: Evidence for general instability of past climate from a 250-kyr ice-core record. *Nature,* **364,** 218–220.

De Boer, A. M., and D. Nof, 2004a: The exhaust valve of the North Atlantic. *J. Climate,* **17,** 417–422.

——, and ——, 2004b: The Bering Strait's grip on the Northern Hemisphere climate. *Deep-Sea Res. I,* **51,** 1347–1366.

Delworth, T. L., S. Manabe, and R. J. Stouffer, 1993: Interdecadal variations of the thermohaline circulation in a coupled ocean–atmosphere model. *J. Climate,* **6,** 1993–2011.

Ditlevsen, P. D., M. S. Kristensen, and K. K. Andersen, 2005: The recurrence time of Dansgaard–Oeschger events and limits on the possible periodic component. *J. Climate,* **18,** 2594–2603.

Duplessy, J. C., N. J. Shackleton, R. G. Fairbanks, L. Labeyrie, D. Oppo, and N. Kallel, 1988: Deepwater source variations during the last climatic cycle and their impact on the global deepwater circulation. *Paleoceanography,* **3,** 343–360.

Ganachaud, A., and C. Wunsch, 2000: Improved estimates of global ocean circulation, heat transport and mixing from hydrographic data. *Nature,* **408,** 453–457.

Goosse, H., J. M. Campin, T. Fichefet, and E. Deleersnijder, 1997: Sensitivity of a global ice–ocean model to the Bering Strait throughflow. *Climate Dyn.,* **13,** 349–358.

Grootes, P. M., M. Stuiver, J. W. C. White, S. Johnsen, and J. Jouzel, 1993: Comparison of oxygen isotope records from the GISP2 and GRIP Greenland ice cores. *Nature,* **366,** 552–554.

Hasumi, H., 2002: Sensitivity of the global thermohaline circulation to interbasin freshwater transport by the atmosphere and the Bering Strait throughflow. *J. Climate,* **15,** 2516–2526.

Heinrich, H., 1988: Origin and consequences of cyclic ice rafting in the Northeast Atlantic Ocean during the past 130,000 years. *Quat. Res.,* **29,** 142–152.

Hemming, S. R., 2004: Heinrich events: Massive late Pleistocene detritus layers of the North Atlantic and their global climate imprint. *Rev. Geophys.,* **42,** RG1005, doi:10.1029/2003RG000128.

——, G. C. Bond, W. S. Broecker, W. D. Sharp, and M. Klas-Mendelson, 2000: Evidence from $^{40}Ar/^{39}Ar$ ages of individual hornblende grains for varying Laurentide sources of iceberg discharges 22 000 to 10 500 yr B.P. *Quat. Res.,* **54,** 372–383.

Hu, A., 2001: Changes in the Arctic and their impact on the oceanic meridional overturning circulation. Ph.D. dissertation, University of Miami, 171 pp.

——, and G. A. Meehl, 2005a: Bering Strait throughflow and the thermohaline circulation. *Geophys. Res. Lett.,* **32,** L24610, doi:10.1029/2005GL024424.

——, and ——, 2005b: Reasons for a fresher northern North Atlantic in the late 20th Century. *Geophys. Res. Lett.,* **32,** L11701, doi:10.1029/2005GL022900.

——, ——, and W. Han, 2004: Detecting thermohaline circulation changes from ocean properties in a coupled model. *Geophys. Res. Lett.,* **31,** L13204, doi:10.1029/2004GL020218.

——, ——, and ——, 2007a: Role of the Bering Strait in the thermohaline circulation and abrupt climate change. *Geophys. Res. Lett.,* **34,** L05704, doi:10.1029/2006GL028906.

——, ——, and ——, 2007b: Causes of a fresher, colder northern North Atlantic in late 20th century in a coupled model. *Prog. Oceanogr.,* **73,** 384–405.

Huang, R. X., and R. W. Schmitt, 1993: The Goldsbrough–Stommel circulation of the world oceans. *J. Phys. Oceanogr.,* **23,** 1277–1284.

Hughes, T. M. C., and A. J. Weaver, 1994: Multiple equilibria of an asymmetric two-basin ocean model. *J. Phys. Oceanogr.,* **24,** 619–637.

Kiehl, J. T., and P. R. Gent, 2004: The Community Climate System Model, version two. *J. Climate,* **17,** 3666–3682.

Krebs, U., and A. Timmermann, 2007: Fast advective recovery of the Atlantic meridional overturning circulation after a Heinrich event. *Paleoceanography,* **22,** PA1220, doi:10.1029/2005PA001259.

Levermann, A., A. Griesel, M. Hofmann, M. Montoya, and S. Rahmstorf, 2005: Dynamic sea level changes following changes in the thermohaline circulation. *Climate Dyn.,* **24,** 347–354.

Manabe, S., and R. J. Stouffer, 1988: Two stable equilibria of a coupled ocean–atmosphere model. *J. Climate,* **1,** 841–866.

Marchitto, T. M., Jr., D. W. Oppo, and W. B. Curry, 2002: Paired benthic foraminiferal Cd/Ca and Zn/Ca evidence for a greatly increased presence of Southern Ocean Water in the glacial North Atlantic. *Paleoceanography,* **17,** 1038, doi:10.1029/2000PA000598.

McCartney, M. S., and L. D. Talley, 1984: Warm-to-cold water conversion in the northern North Atlantic Ocean. *J. Phys. Oceangr,* **14,** 922–935.

McManus, J. F., R. Francois, J.-M. Gherardi, L. Keigwin, and S. Brown-Leger, 2004: Collapse and rapid resumption of Atlantic meridional circulation linked to deglacial climate changes. *Nature,* **428,** 834–837.

Meehl, G. A., and Coauthors, 2007: Global climate projections. *Climate Change 2007: The Physical Science Basis,* S. Solomon et al., Eds., Cambridge University Press, 747–845.

Mikolajewicz, U., and E. Maier-Reimer, 1994: Mixed boundary conditions in ocean general circulation models and their influence on the stability of the model's conveyor belt. *J. Geophys. Res.,* **99,** 22 633–22 644.

Ohlmann, J. C., 2003: Ocean radiant heating in climate models. *J. Climate,* **16,** 1337–1351.

Otto-Bliesner, B. L., E. C. Brady, G. Clauzet, R. Tomas, S. Levis, and Z. Kothavala, 2006: Last Glacial Maximum and Holocene climate in CCSM3. *J. Climate,* **19,** 2526–2544.

——, C. D. Hewitt, T. M. Marchitto Jr., E. C. Brady, A. Abe-Ouchi, M. Crucific, S. Murakami, and S. L. Weber, 2007: Last Glacial Maximum ocean thermohaline circulation: PMIP2 model intercomparisons and data constraints. *Geophys. Res. Lett.,* **34,** L12707, doi:10.1029/2007GL029475.

Overland, J. E., and A. T. Roach, 1987: On northward flow in the Bering and Chukchi seas. *J. Geophys. Res.,* **92,** 7097–7105.

Peltier, W. R., and L. P. Solheim, 2004: The climate of the Earth at Last Glacial Maximum: Statistical equilibrium state and a mode of internal variability. *Quat. Sci. Rev.,* **23,** 335–357.

Pflaumann, U., and Coauthors, 2003: Glacial North Atlantic: Sea-surface conditions reconstructed by GLAMAP 2000. *Paleoceangraphy,* **18,** 1065, doi:10.1029/2002PA000774.

Rahmstorf, S., 1995: Bifurcations of the Atlantic thermohaline circulation in response to changes in the hydrological cycle. *Nature,* **378,** 145–149.

——, 1996: On the freshwater forcing and transport of the Atlantic thermohaline circulation. *Climate Dyn.,* **12,** 799–811.

——, 2002: Ocean circulation and climate during the last 120,000 years. *Nature,* **419,** 207–214.

——, and Coauthors, 2005: Thermohaline circulation hysteresis: A model intercomparison. *Geophys. Res. Lett.,* **32,** L23605, doi:10.1029/2005GL023655.

Reason, C. J. C., and S. B. Power, 1994: The influence of the Bering Strait on the circulation in a coarse resolution global ocean model. *Climate Dyn.,* **9,** 363–369.

Roche, D., D. Paillard, and E. Cortijo, 2004: Constraints on the duration and freshwater release of Heinrich event 4 through isotope modelling. *Nature,* **432,** 379–382.

Sarnthein, M., and Coauthors, 1995: Variations in Atlantic surface ocean paleoceanography, 50°–80°N: A time-slice record of the last 30,000 years. *Paleoceanography,* **10,** 1063–1094.

Schmittner, A., 2005: Decline of the marine ecosystem caused by a reduction in the Atlantic overturning circulation. *Nature,* **434,** 628–633.

Shaffer, G., and J. Bendtsen, 1994: Role of the Bering Strait in controlling North Atlantic ocean circulation and climate. *Nature,* **367,** 354–357.

Seidov, D., and B. J. Haupt, 2003: Freshwater teleconnections and ocean thermohaline circulation. *Geophys. Res. Lett.,* **30,** 1329, doi:10.1029/2002GL016564.

——, and ——, 2005: How to run a minimalist's global ocean conveyor. *Geophys. Res. Lett.,* **32,** L07610, doi:10.1029/2005GL022559.

——, M. Sarnthein, K. Stattegger, R. Prien, and M. Weinelt, 1996: North Atlantic ocean circulation during the last glacial maximum and subsequent meltwater event: A numerical model. *J. Geophys. Res.,* **101,** 16 305–16 332.

Sidall, M., E. J. Rohling, A. Almogi-Labin, Ch. Hemleben, D. Meischner, I. Schmelzer, and D. A. Smeed, 2003: Sea-level fluctuations during the last glacial cycle. *Nature,* **423,** 853–858.

Smith, L. T., E. P. Chassignet, and R. Bleck, 2000: The impact of lateral boundary conditions and horizontal resolution on North Atlantic water mass transformations and pathways in an isopycnic coordinate ocean model. *J. Phys. Oceanogr.,* **30,** 137–159.

Stocker, T. F., 2002: North-south connections. *Science,* **297,** 1814–1815.

——, and D. G. Wright, 1991: Rapid transitions of the ocean's deep circulation induced by changes in surface water fluxes. *Nature,* **351,** 729–732.

Stommel, H., 1961: Thermohaline convection with two stable regimes of flow. *Tellus,* **13,** 224–241.

Stouffer, R. J., and Coauthors, 2006: Investigating the causes of the response of the thermohaline circulation to past and future climate changes. *J. Climate,* **19,** 1365–1387.

Talley, L. D., J. L. Reid, and P. E. Robbins, 2003: Data-based meridional overturning streamfunctions for the global ocean. *J. Climate,* **16,** 3213–3226.

Thorpe, R. B., J. M. Gregory, T. C. Johns, R. A. Wood, and J. F. B. Mitchell, 2001: Mechanisms determining the Atlantic thermohaline circulation response to greenhouse gas forcing in a non-flux-adjusted coupled climate model. *J. Climate,* **14,** 3102–3116.

Timmermann, A., M. Latif, R. Voss, and A. Grötzner, 1998: Northern Hemispheric interdecadal variability: A coupled air–sea mode. *J. Climate,* **11,** 1906–1931.

——, S.-I. An, U. Krebs, and H. Goosse, 2005a: ENSO suppression due to weakening of the North Atlantic thermohaline circulation. *J. Climate,* **18,** 3122–3139.

——, U. Krebs, F. Justino, H. Goosse, and T. Ivanochko, 2005b: Mechanisms for millennial-scale global synchronization during the last glacial period. *Paleoceanography,* **20,** PA4008, doi:10.1029/2004PA001090.

Vellinga, M., R. A. Wood, and J. M. Gregory, 2002: Processes governing the recovery of a perturbed thermohaline circulation in HadCM3. *J. Climate,* **15,** 764–779.

Wadley, M. R., and G. R. Bigg, 2002: Impact of flow through the Canadian Archipelago and Bering Strait on the North Atlan-

tic and Arctic circulation: An ocean modelling study. *Quart. J. Roy. Meteor. Soc.,* **128,** 2187–2203.

Weaver, A. J., and T. M. C. Hughes, 1992: Stability and variability of the thermohaline circulation and its links to climate. *Trends Phys. Oceanogr.,* **1,** 15–70.

Weber, S. L., and Coauthors, 2007: The modern and glacial overturning circulation in the Atlantic ocean in PMIP coupled model simulations. *Climate Past,* **3,** 51–64.

Wijffels, S. E., R. W. Schmitt, H. L. Bryden, and A. Stigebrandt, 1992: Transport of freshwater by the oceans. *J. Phys. Oceanogr.,* **22,** 155–162.

Woodgate, R. A., and K. Aagaard, 2005: Revising the Bering Strait freshwater flux into the Arctic Ocean. *Geophys. Res. Lett.,* **32,** L02602, doi:10.1029/2004GL021747.

Yokoyama, Y., K. Lambeck, P. De Deckker, P. Johnston, and L. K. Fifield, 2000: Timing of the Last Glacial Maximum from observed sea-level minima. *Nature,* **406,** 713–716.

Yu, E.-F., R. Francois, and M. P. Bacon, 1996: Similar rates of modern and last-glacial ocean thermohaline circulation inferred from radiochemical data. *Nature,* **379,** 689–694.

Zhang, R., and T. Delworth, 2005: Simulated tropical response to a substantial weakening of the Atlantic thermohaline circulation. *J. Climate,* **18,** 1853–1860.